Int J Adv Manuf Technol (2015) 81:935–953
DOI 10.1007/s00170-015-7081-7

ORIGINAL ARTICLE

Dynamic precision control in single-grit scratch tests using acoustic emission signals

James Marcus Griffin[1] · **Fernando Torres**[2]

Received: 15 October 2014 / Accepted: 23 March 2015 / Published online: 15 May 2015

Abstract Acoustic emission (AE) is very sensitive to minuscule molecular changes which allow it to be used in a dynamic control manner. The work presented here specifically investigates approaching grit and workpiece interaction during grinding processes. The single grit (SG) tests used in this work display that the intensities from air, occurring in between the grit and workpiece, show an increasing intensity as the grit tends towards the workpiece with 1-μm increments. As the grit interacts with the workpiece, a scratch is formed; different intensities are recorded with respect to a changing measured depth of cut (DOC). In the first instance, various AE were low tending towards high signal to noise ratios which is indicative of grit approaching contact; when contact is made, frictional rubbing is noticed, then ploughing with low DOC and, finally, actual cutting with a higher associated DOC. Dynamic control is obtained from the AE sensor extracting increasing amplitude significant of elastic changing towards greater plastic material deformation. Such control methods can be useful for grinding dressing ratios as well as achieving near optimal surface finish when faced with difficult to cut geometries. Two different materials were used for the same SG tests (aerospace alloys: CMSX4 and titanium-64) to verify that the control regime is robust and not just material dependent. The AE signals were then classified using neural networks (NNs) and classification and regression trees (CART)-based rules. A real-time simulation is provided showing such interactions allowing dynamic micro precision control. The results show clear demarcation between the extracted synthesized signals ensuring high accuracy for determining different phenomena: 3–1 μm approaching touch, touch, slight plastic deformation and, increasing plastic deformation. In addition to dressing ratios, the results are also important for micron accuracy set-up considerations.

Keywords Acoustic emission · Feature extraction · Precision control · Single-grit scratch · CART · Neural networks · Simulations · Embedded controllers

Nomenclature

AE	Acoustic emission
C	Cutting
DOC	Depth of cut
DSP	Digital signal processing
FFT	Fast Fourier transform
NN	Neural network
P	Ploughing
R	Rubbing
STFT	Short-time Fourier transform
SG4/SG	Single-grit trial 4/single grit
T210-T212	Test 210-test 212
T51-T54	Test 51-test 54
CART	Classification and regression trees

1 Introduction

When carrying out precision machining, there is a need to control processes through various feedback signals that should be both accurate and sensitive to change. A sensor technology that can be applied is that of acoustic emission (AE) extraction. With such sensitive characteristics and its lack of standarisation, there is a need to calibrate AE to other standarised energy quantities or

✉ James Marcus Griffin
james.griffin2@coventry.ac.uk

[1] Faculty of Engineering and Computing,
Engineering and Computing Building,
Coventry University,
Gulson Road, Coventry, CV1 2JH, UK

[2] Fablab, Department of Mechanical Engineering,
School of Physical and Mathematical Sciences,
Beauchef 851, University of Chile,
Santiago de Chile, 8370456, Chile

daily calibrate against a reference phenomenon with a relatively constant energy pattern, such as the breaking of a graphite fibre pencil [1]. This was carried out during previous work [2] where AE, sensitive to minute material interactions, were correlated to force measurements. The force gives verification against AE where measurements can differ significantly on a daily basis. Such differences are apparently due to environmental conditions, differences in material characteristics and the different applied stresses for fracture to occur. The method presented in this work looks at accurate correlation of approaching touch; such intensities increase as the grit gets closer to the workpiece (last 3 μm the growing phenomenon was noticed), surface touch (significant to the rubbing phenomenon), slight plastic deformation (significant to the ploughing phenomenon) with low depth of cut (DOC) and, finally, plastic deformation with higher DOC (significant to the cutting phenomenon). From such energy correlations, it is possible to control processes within submicron accuracy.

Force sensors are very useful for extracting workpiece deflection and even stiffness characteristics; however, using the force alone will only confirm the different levels of intensities relating to touch and touch tending towards plastic deformation and not that of approaching touch. Both AE and force sensors look at similar conditions within the machining environment, but force signals are used to verify AE in terms of slight touch tending towards increasing plastic deformation. Discussions will be made regarding certain limiting conditions that have to be taken into consideration when carrying out miniscule grit to workpiece interactions such as those seen in single-grit (SG) scratch tests.

Another important point to highlight is that the force sensor requires more calibration time using standard weights and, furthermore, requires fixture to the workpiece. On the other hand, AE sensors can be fixed on by glue giving access to difficult and inaccessible places.

The work presented in [3] looks at direct control where the power signal is used for identifying when a change of tool should take place. Again, power signals can give different facets of information, where a rapid increase in peak energy at a particular time interval can be significant to part/tool breakage and, at the same time, give information to the location of the tool's malfunction, however, only increases are found from contact and not that of approaching contact. The power sensed signal is somewhat similar to that of AE as they are both measuring energies, albeit it is a non-invasive extraction technique; so power can be used in conjunction with AE as opposed to AE and force, where force is invasive from the set-up perspective. Force and power only verify the growing plastic deformation and not that of approaching touch; thus, only AE can be used for this.

The main investigation objectives are:

- Characterise the different levels of phenomena: approaching touch, touch, slight plastic deformation (DOC <0.5 μm) and plastic deformation (DOC ≥0.5 μm).
- Characterise the phenomena using both the time and short-time Fourier transform (STFT) of the AE-extracted signal correlated to horizontal SG scratch tests.
- Summarise the extracted information.
- Apply the procedure on two different materials: CMSX4 and Titanium-64.
- Verify such signals with dual AE sensors, set at equal distances apart and, from sensor delay, determine the position of phenomena interaction.
- Classify different levels of the characterised phenomena.
- Produce a real-time simulation displaying changing energy patterns as the grit tends towards higher DOC from near touch.

The remainder of this paper is organised as follows: first, AE technology used for precision machining is introduced, followed by an introduction to classifier technologies. CART is then discussed for controlling precision machining with neural networks (NN) as the second verification. Then the experimental set-up followed by AE-extracted signals and SG analysis. For the final part, a simulation is presented using both classifiers for possible embedded employment and finally, the conclusions.

2 AE technology used for precision machining

There is no recorded work to date that discusses AE used for controlling the approaching and actual increasing contact; however, other work using AE can be seen in monitoring tool wear with the addition of force signals, where both are introduced to a supervised back-propagated ART-NN to distinguish salient AE fast Fourier transform (FFT) features experienced during turning insert tool wear [4]. Jemielniak investigates this further by correlating AE measurements and insert wear, promoting more generalised learning capabilities with adaptive biases between both training and test data ensuring the NN does not get stuck in local minima [5]. Other work investigates wavelet transforms (WT) with a fuzzy-NN to determine the wear states from correlated AE during drilling of 40Cr steel [6]. The insert wear mechanism has a defined cutting edge and can partially represent the mechanism of SG cutting seen in grinding scratch tests. The work presented in [7] predicts insert wear through NN models using the input of time, where velocity, feed rate and cutting force. Such work is useful for the one discussed in this paper due to the parallels between SG and insert technology simulation models. Not to mention that the work is correlated with minute phenomena, and during a machining process, there are many facets of information which can be used for different control considerations. In [8], the estimation of cutting forces is used to estimate the surface roughness for hard turning. When looking at SG micro mechanics, some signals and material phenomenon distinguish patterns in the surface roughness, namely rubbing or rubbing with slight plastic deformation. From discussing other literature, there is a direct relationship between

force and AE, especially for verification of such small phenomenon, which is of particular interest to the work presented here.

Investigations shown in [9] look at wear mechanisms experienced during micro-milling, which quantifies how AE can be used to distinguish such microscopic phenomena. [10] and [11] investigates other precision machining processes where fuzzy identification using extended subtractive cluster analysis and least squares gives an adaptive filter capability that, when tuned, can accurately measure material removal rates, giving the process more accuracy against unwanted noise. The research discussed in this paper utilises such ideas in identifying microscopic features through experienced AE signals when the grit approaches touch and touch with greater workpiece interaction, generating plastic deformation. Moreover, the precision of AE technologies applied to wear can also be translated for measuring the distance between the tool tip and the workpiece; this is important when considering micromachining operations. If the AE is post-processed in a computationally affordable fashion, such salient information can be used to control the distance in real-time and to accurate levels.

The research presented in [12] is of particular interest as it uses NN for the control of deviation errors based on the AE measurements of flank tool wear when turning. This is where vibrations give a trace to deviations away from the specific CNC programme. These deviation errors are attributed to various parameters, such as a change in temperature, significant to increased flank tool wear and, actuator backlash errors. The work presented here aims to give a capability and be able to do the same for the grinding perspective in controlling deviation errors based on identified distances. Also, by using this sensed feedback, deviation errors from various machining phenomena can be corrected by correlating the sensed distance with the obtained CNC positioning.

AE is being increasingly used in industry due to the possibilities to measure a change in minute phenomena. However, as a robust calibration method for such developing technologies have not yet been accepted in terms of standarisation, so far only best practices are being used [13]. Reciprocity calibration have also been used in [1] for underwater acoustics, and both Raleigh and longitudinal waves were measured from the AE event. This is also summarised in [1], where spurious waves do not make a huge significance to dominant waves (Raleigh and longitudinal). In short, the AE elastic waves are located in terms of the dominant energy bands.

In terms of using the calibrated AE data in a control capacity, [14] investigates how the classifiers *k*-means and self-organising maps (SOM) were used in segregating different material failure reference tensile tests and recorded AE signatures. Such AE is reduced in *n*-dimensionality to give rise time, peaks and counts. A similar process is applied here to reduce the obtained time-extracted AE signals, as well as the reduced time–frequency information. Where research discussed here uses, windows of 300 points calculating maximum, minimum and kurtosis of the presented STFT signal features. These summaries are described graphically in Fig. 20 looking at the computed parallel coordinates; note that the more elastic deformation phenomena are more significant when compared with the plastic deformation phenomena due to much larger time steps associated for emitted, less intensive energy phenomena.

Using the raw extracted time and translated time–frequency signal affords the user a very powerful input for working in both real time and with good accuracy. Such control regimes require the extension of using statistics to provide the salient points which are significant for an expert controller to react to, such as those seen by NNs and CART rules.

FFT have been used for condition monitoring in the past; however, it does not give any time information of when the event occurred, which is fundamental to the very nature of spontaneously released transient elastic energy; instead, FFT calculates the average frequency over the duration of the extracted signal and can be applied to a non-stationary AE signal, but it will not describe the transient phenomena in terms of frequency resolution [15].

Instead, STFT allows observability in both time and frequency domains by calculating FFT on equally spaced intervals designated across the raw extracted time signal. There is a trade-off between frequency and time resolution, which is needed to accurately distinguish features in a noisy environment. That said, STFT still offers enough resolution when required to characterise an AE signal for precision control amongst other micro grinding phenomena [2].

For the work presented here, the time information is first reduced in terms of max peak, back burst time to zero from the identified max peak and kurtosis of the corresponding peak. This is carried out for a given time interval (in this case significant to 300 points, which was considered a good signal window catering for the miniscule and the less miniscule) for five maximum and five minimum peaks. This rich salient data is then used for the classification of different energies experienced during approaching and the actual interaction between the grit and workpiece. Additionally, a STFT is taken from the same interval from where ten max points are taken in terms of frequency and amplitude to be concatenated to the already summarised time data and then input to the classifier.

3 Classifier technologies for intelligent control of 1-μm accuracies

The following section looks at the classification of micron precision phenomena for 1-μm accuracies. The two classification techniques chosen are CART and NNs, where both classifiers together give a robust account against outliers and, potential unwanted signal noise. Firstly, CART is introduced followed by NN.

3.1 CART rule-based system for precision control

CART is a classification method similar to fuzzy clustering, very useful in segregating *n*-dimensional data sets with the added facet over most other classifiers: it produces transparent rules. In addition, its suitability to handle *n*-dimensional data is to be taken into account, especially considering that real-time, computationally expensive, data reduction techniques are unsuitable.

CART builds classification and regression trees for predicting continuous dependent variables (regression) and categorical predictor variables (classification) [16]. It achieves its functionality by recursively splitting the feature space into sets of non-overlapping regions and by predicting the most likely value of the dependent variable with each region. By generating a binary tree through recursive partitioning, it splits the data into sub-nodes based on the minimisation of a heterogeneity criterion computed at the resulting sub-nodes. With the CART algorithm, the tree is forwardly propagated, using forward stepwise regression, for best purity of node split. The best node split becomes the chosen value of partition (see Eq. 1).

A good splitting criterion is

$$\mathrm{PRE} = \Phi(s,t)$$

where PRE is the minimum production reduction error and s is the split at any node t. The best purity measure looks at the best unique minimal classification where impure would be to have many unnecessary classes. For the CART algorithm, the accuracy percentage of classification is used as the best purity measure.

Misclassification error:

$$Q_m = \frac{1}{N_m} \sum_{x_i \in R^m} (y_i \neq k(m)) = 1 - P_{mk(m)} \tag{1}$$

where y_i is the output of the individual under test and *k(m)* is the class category under test.

This method of classification is chosen because the tree fitting methods are actually closely related to cluster analysis [17]. This is where each node can be thought as a cluster of objects, or cases, that are split by further branches in the tree. Note that the top node covers the whole sample set and each remaining node contains a subset of the original sample, and so on as the split level increases [18].

A classification tree represents a set of nested logical if–then conditions (similar to a decision rule-based system) for the values of the feature variables, which allows the prediction of the corresponding class.

CART can handle missing values by imputing such values in obtaining the mean over the complete observations. The produced CART model can be tested on a separately specified test set. Additionally, the model can be saved and used subsequently on additional test sets. The rules can be transferred into a system to work as an embedded controller. Note that the same dataset size has to be applied to the classifier; if a problem exists with the data, then zero padding is necessary for introduction into the classifier.

Some points for discussion on best tree representations are as follows:

- A very large tree may over fit the data.
- A small tree might not capture the important structure.

Therefore, there is a trade-off consideration for the best tree when thinking of the overall size:

- The optimal tree size should be adaptively chosen from the data provided.
- Different stopping criteria can give different results, such as when an impurity threshold is reached and the branching and splitting is halted or a specified minimum of branch level is achieved.
- Think of a pruning strategy that does not impact on the overall tree classification accuracy.

3.1.1 Advantages of tree-based methods

Tree-based classifiers can cater for both categorical and ordered variables in a simple and natural way. Automated stepwise variable selection with built-in complexity reduction ensures powerful and compact rules are found. CART provides estimates for query samples based on the misclassification rates, which gives the technique further confidence in its ability to accurately classify. Tree-based methods are invariant under all monotone transformations for the individual ordered variables. Such a paradigm is also robust to outliers and misclassified points based on the training set. Finally, one of the important reasons for being used here is its ability to give easy to interpret outputs.

3.1.2 Limitations of tree-based methods

One important consideration is the high variance of output based on its hierarchical nature to classify. A small change in data may result in different splits, thus making such interpretations precautious. Errors are made from the top node filter all the way down to the lower nodes. Such limitations have been reduced based on bagging averages and using random forest techniques. All tests carried out using this technique were verified against test and unseen verification data sets. With high classifications, added confidence in terms of accumulated accuracy is achieved.

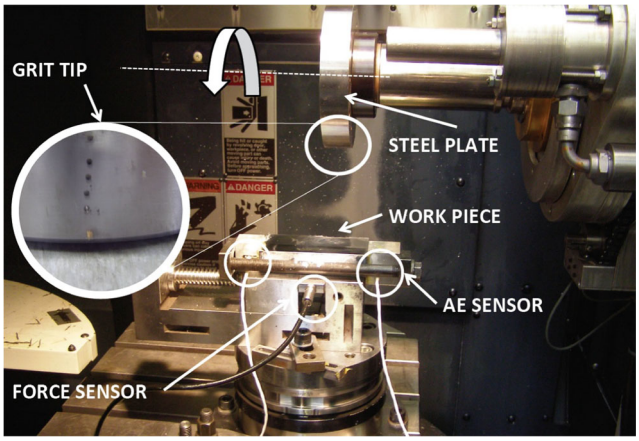

Fig. 1 Ti64 experimental set-up in Makino A55 Machine Centre

3.2 NN for precision control

A large number of researchers have reported the application of using NN models for the classification of phenomena of interest when applied to tool condition monitoring ([19] and [20]). Feed-forward NN models have been used for pattern recognition in image analysis and sound waves signal analysis. The NN consists of a complex interconnection of units which are also known as nodes or neurons. The general layout consists of a set of neuron layers linked together through complex connections. Such layout and features are known as the network topology. This is applied to the extracted AE signals for the classification of precision phenomena over cutting, ploughing, rubbing and the most important for dynamic control: approaching touch.

A multilayer NN is required due to the complexity of the data presented as summarised pre-processed signal data. This type of data is not only non-linear but also *n*-dimensional.

The output of each neuron is a function of its inputs. Specifically, the output of the *j*th is described by Eqs. 2 and 3:

$$U_j = \sum \left(P_i \cdot w_{ij}\right) \tag{2}$$

$$a_i = F\left(U_j + t_j\right) \tag{3}$$

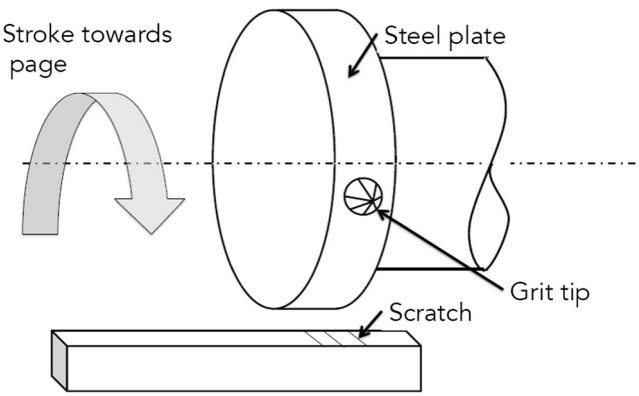

Fig. 2 Sketch of horizontal scratch test rig

For every neuron *j* in a layer, each of the inputs P_i to that layer is multiplied by a previously established weight w_{ij}. These are all summed together, resulting in an internal value U_j of the operation. This value is then biassed by a previously established threshold value t_j and sent through an activation function $F()$ (which can be either linear on non-linear), giving that neuron an output P_j. This is done recursively until the output nodes are reached, giving the NN output a_i.

Equation 4 describes the output error obtained from each neuron:

$$\mathrm{ME} = \frac{1}{\Omega}\sum_{i=1}^{\Omega}\left(t_i - a_i\right)^2 \tag{4}$$

where ME is the mean squared error and a_i is the *i*th output of the network. The error function can be applied to the NN in a batch training fashion at the end of the whole data presentation or sequentially after each input–output pair.

For the back propagation algorithm, the weight and bias update equations are as follows:

$$\Delta w_{ij}^k = \alpha \cdot \frac{\partial ME}{\partial w_{ij}^k} \tag{5}$$

$$\Delta b_i^k = \alpha \cdot \frac{\partial ME}{\partial b_i^k} \tag{6}$$

where α is the learning rate, whose value has a trade-off to ensure it is small enough to gain a true convergence, but large enough to separate the data space in adequate time. Eqs. 5 and 6 are iteratively changed across the network along with other functions to provide learning sensitivity. This process of weight and input, and error calculation propagates through the NN to provide the segregation rules which separates the data according to class (target vector). The *b* is a bias term used to influence the training weights for NN training.

4 Experimental set-up

This paper obtains its results from a near noise-free environment; however, as previous research has displayed [21], with the use of filters, such signals obtained during harsh environment can achieve good signal to noise ratios. Then they can be calibrated against known signals and used for monitoring the onset and the continuation of material failure. The work presented here uses a number of different signals obtained during various experimental trials.

The proposed work outlined in this paper is based on work discussed by [2], where intelligent correlation is made from the signal input/output to the classifier system which essentially is a CART set of rules and a four-layer NN (two hidden layers to cater for the presented non-linear data).

Table 1 Summary of the CMSX4 and Ti64 aerospace materials

Property	CMSX4	Titanium-64
Composition (WT%)	Mo: 0.6, Cr: 7.0, Ti: 1.0, Al: 5.6, Co: 10, Ni: 67, Re: 3.0, W: 6.0	C: 0.08, Al: 5.50–6.75, Fe: 0.30, H: 0.01
Density (kg/m^3)	8690	4650
Hardness (HV)	520	349
Tensile strength (Mpa)	1090	950
Yield strength (Mpa)	990	880
Elastic modulus (Gpa)	18.5	109.6
Elongation (%)	10–12	14
Melting point (°C)	1395	1604
Poisson's ratio	0.273	0.34
Thermal conductivity (W/mK)	12–63	6.7

The experiment carried out for this work consisted of SG tests (see Figs. 1 and 2 for experimental setup). This is where a grit is glued into a metal plate via a micron drilled hole that is fixed within a rotating spindle and, with 1-μm advancing increments, the SG tends towards the workpiece. Such tests are used to simulate the micro-processes of grinding, giving more information in terms of the low-level material interactions. These tests can be used for controlling micro-machining where AE signatures were achieved in terms of approaching touch, slight touch (significant to rubbing), touch with very low DOC (significant to ploughing) and touch with higher levels of DOC (significant to cutting).

Data collected from these experiments is then reduced in terms of dimensionality and presented to two independent classifiers to carry out expert classification. The SG experiments give both micro-force and AE relationships for such miniscule intensities, which are below and approaching that of pencil fibre break tests.

Two materials were used (see Table 1 for material characteristics) to see if a generic control strategy can be applied to precision machining processes independent of the material properties. Work seen in [2] looks at calibrated AE against force data; however, for precision machining, there is a need to pick up the approaching tool to the workpiece surface. For example, for dressing a micro grinding tool, the DOC are so small that there is a need to notice air/approaching touch and slight touch for initial reference. Only AE sensors are capable of sensing such minute interactions. Force sensors, only give further information based on actual touch, whether that be slight or touch tending towards increasing material plastic deformation.

The experiments displayed in Fig. 1 were designed specifically looking for different intensities between two AE sensors and two different materials.

The SG scratch test experiments were carried out on a specially designed test rig fixed within a Makino A55 Machine Centre as shown in Fig. 1. Aerospace materials CMSX4 and Titanium-64 were used for the SG tests to show classifier robustness where all samples tested were polished to a high surface quality, which increases the tests confidence with respect to precision measurements. Roughness (Ra) across all workpieces was measured between 0.02 and 0.03 μm.

The SG was fixed to the plate in a protruding fashion, which would ensure the SG was the first object to make contact with the workpiece when controlled within a micron of accuracy.

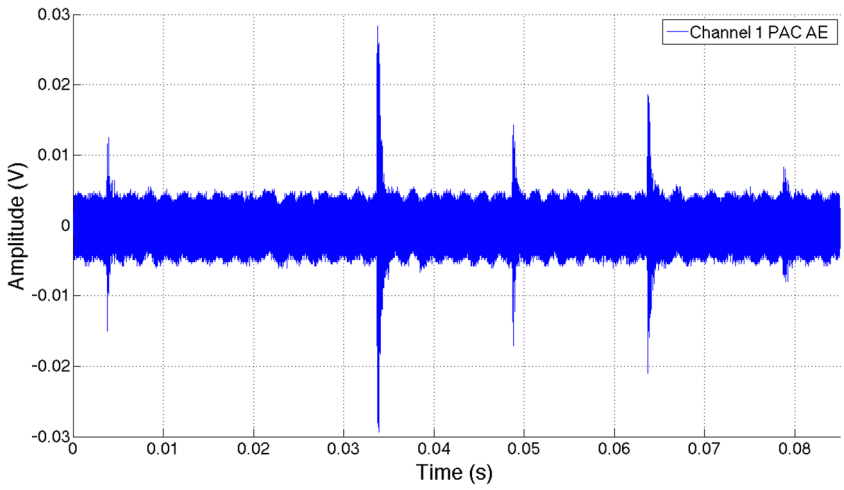

Fig. 3 Raw time for CMSX4 material during SG test 210. Intensities shown correspond to touch and rubbing phenomenon

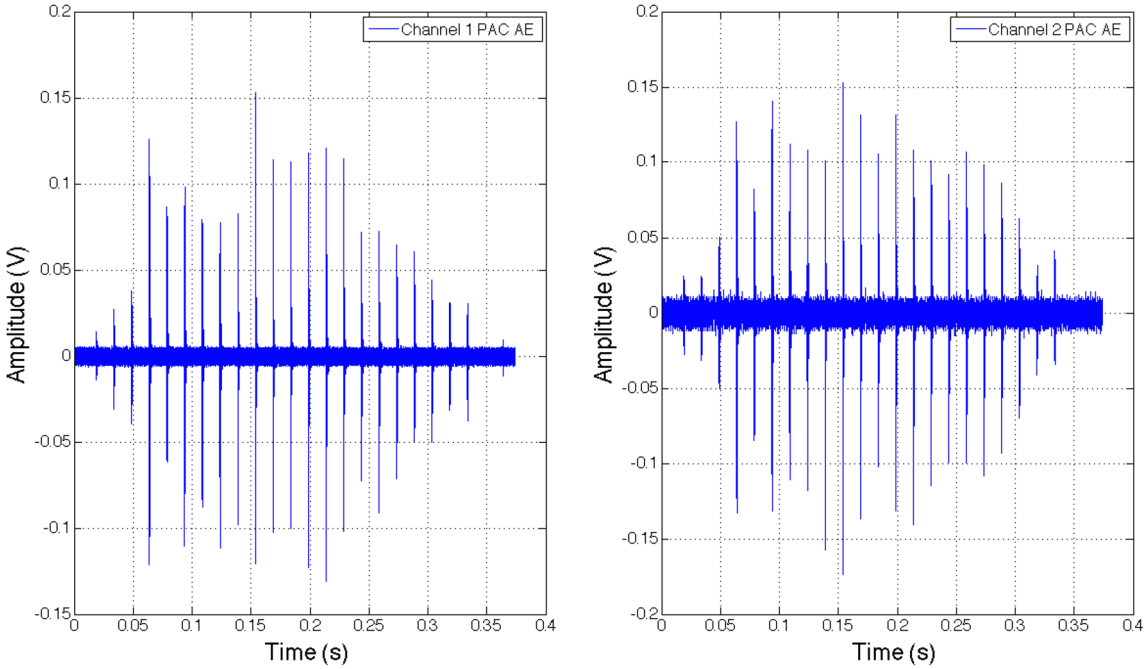

Fig. 4 Raw time signal for CMSX4 material during test 212 showing AE channel 1 (*left*) and AE channel 2 (*right*) for slight touch, touch and higher levels of material interaction with more plastic deformation

The machine set-up consisted of both AE and force sensors being attached in a manner to ensure maximum signal extraction. To provide a sealed medium for AE to vibrate from workpiece/SG to the sensor, grease was applied in between the AE sensor housing and workpiece holder rig. For monitoring the force and AE, two computers were synchronised by switch-driven digital acquisition cards (DACs).

The scratch tests were carried out by feeding a rotating Al_2O_3 grit towards a flat horizontally placed workpiece as shown by Fig. 2. With a micron incremental grit stroke, a scratch groove was formed on the surface of the flat sample. The average scratch depth has about 1 μm, which is a typical value of grinding chip in high-efficiency grinding. The scratching wheel rotational speed is 4000 rpm, with a feed rate of 4000 mm/min under the down grinding condition (see Fig. 2). During a single scratch action, the AE feature frequency bands and intensities change over time. In short, the mechanical AE propagation should be considered in both time and frequency features. However, the prominent AE feature frequencies of the scratches are in the range of 100~550 kHz, which are similar to the AE feature frequencies in grinding tests experienced in previous work [22]. Not only

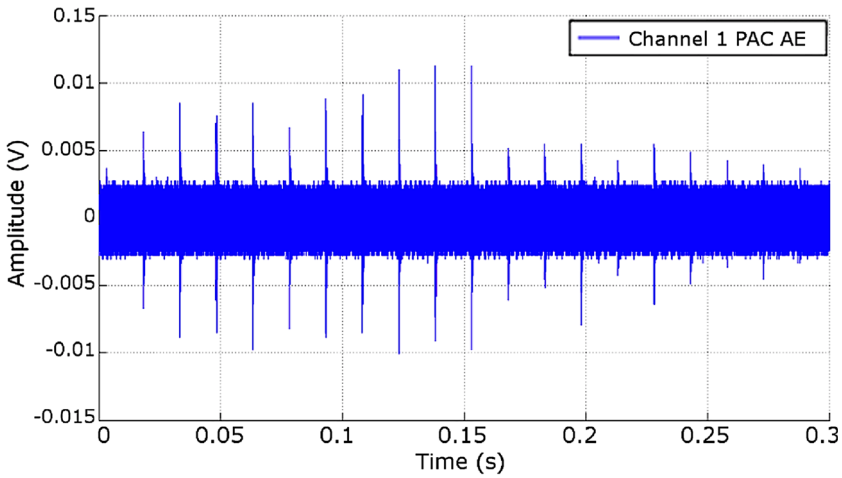

Fig. 5 Raw time signal for Ti64 material during SG test 51

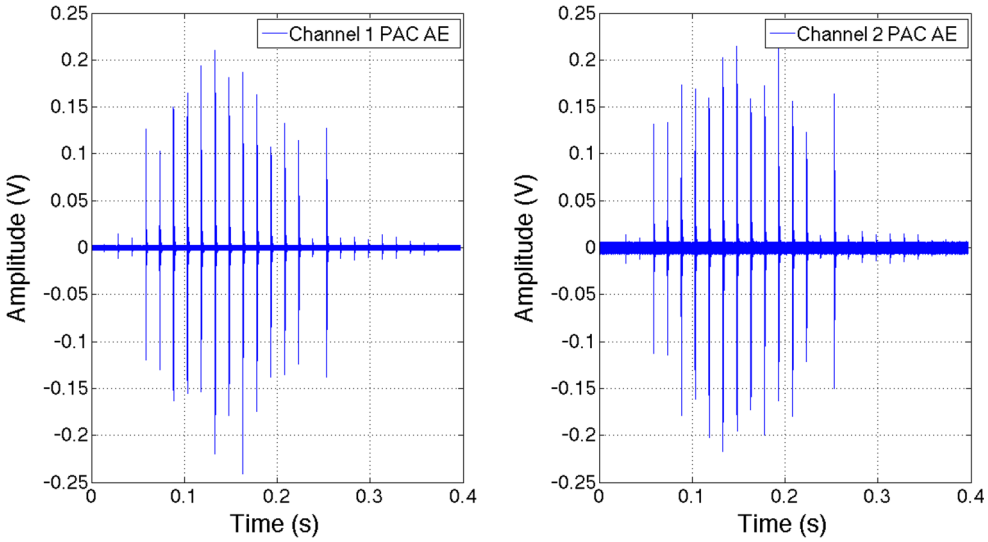

Fig. 6 Raw time signal for Ti64 material during test 54 showing AE channel 1 (*left*) and AE channel 2 (*right*) for slight touch, touch and higher levels of touch with more plastic deformation

the different mechanisms of plastic deformation incur changing frequency bands but also the approaching touch between grit and workpiece as they tend toward each other.

An AE data acquisition system with two identical physical acoustics WD AE (wide band fast response) sensors were used, each with a frequency response range of 80 kHz to 1 MHz. Both sensors were set up at equal distance apart (see Fig. 1). The sampling rate was set to 5 MHz to ensure no aliasing occurred when the signal was reconstructed using the Matlab Signal Toolbox® (digital signal processing (DSP)) and all the short-burst high-frequency information was obtained.

5 AE from SG scratch tests

In this section, the extracted AE signals are examined, where both channels 1 and 2 can be compared against each other (see Figs. 3, 4, 5 and 6).

Looking at Fig. 3, there can be confidence that air and approaching touch is established as the nearer sensor (sensor 1) picks up the slight phenomenon but not the other sensor (sensor 2). There is some pickup of the more intense air and approaching touch, which is picked up by both sensors. However, the further sensor has a lower intensity reading.

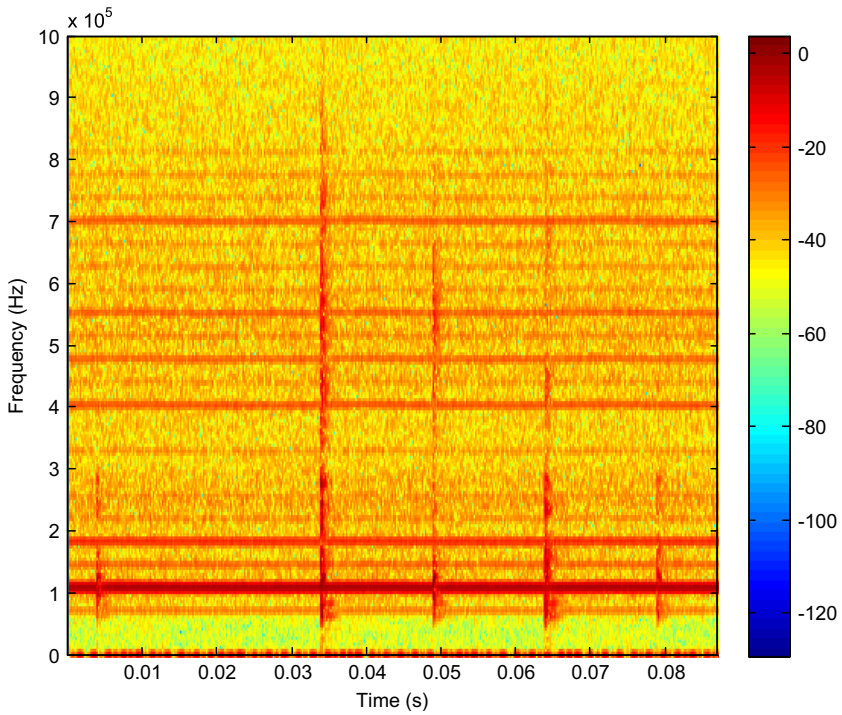

Fig. 7 STFT for CMSX4 material during test 210

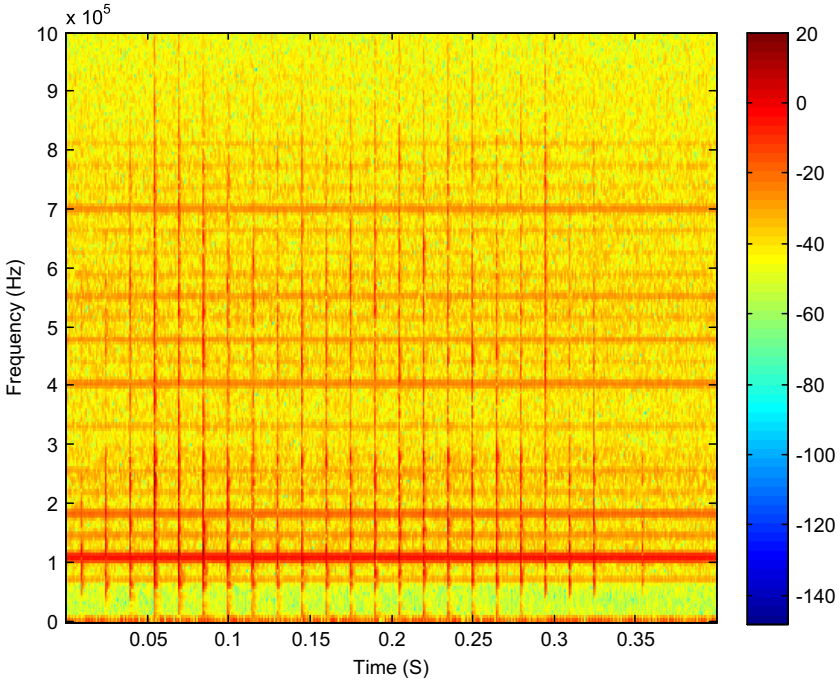

Fig. 8 STFT for CMSX4 material during test 212

Figure 4 displays slight touch and different levels of plastic deformation (significant of increasing DOC). Sensor 1 was verified by sensor 2. Here, the aerospace material CMSX4 is used for such tests.

Figure 5 displays approaching touch cases for the second aerospace material Titanium-64. Here, the material interaction phenomenon was more in a neutral position between both sensors, confirming similar recorded intensities by both AE sensors.

Figure 6 displays the final set of AE-extracted signals, where greater stress of material interactions give a higher intensity in recorded amplitude. Such results, seen with both materials, display how such an idea can be used for precision control during machining processes. The high intensities

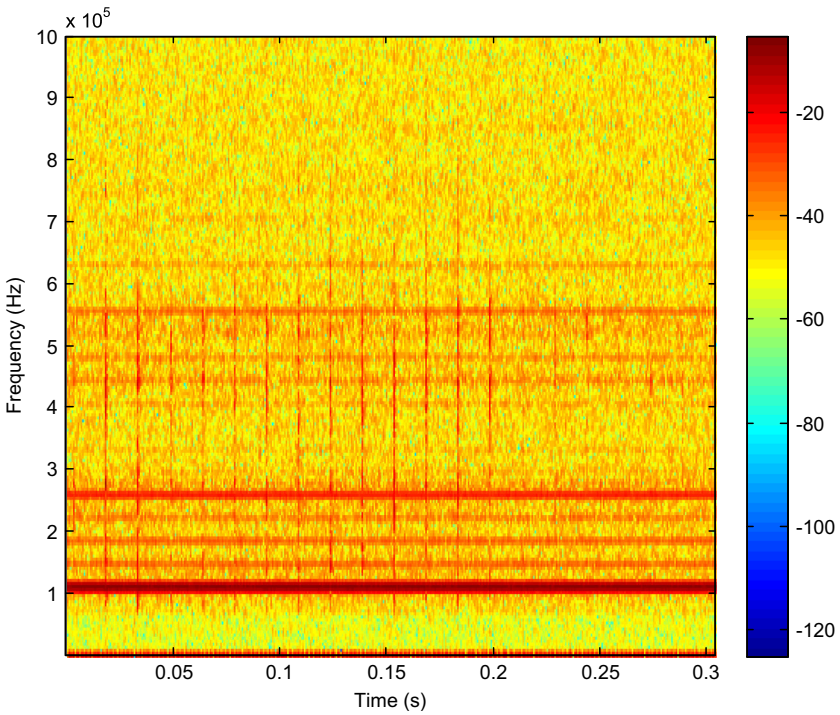

Fig. 9 STFT for the Titanium-64 material during test 51

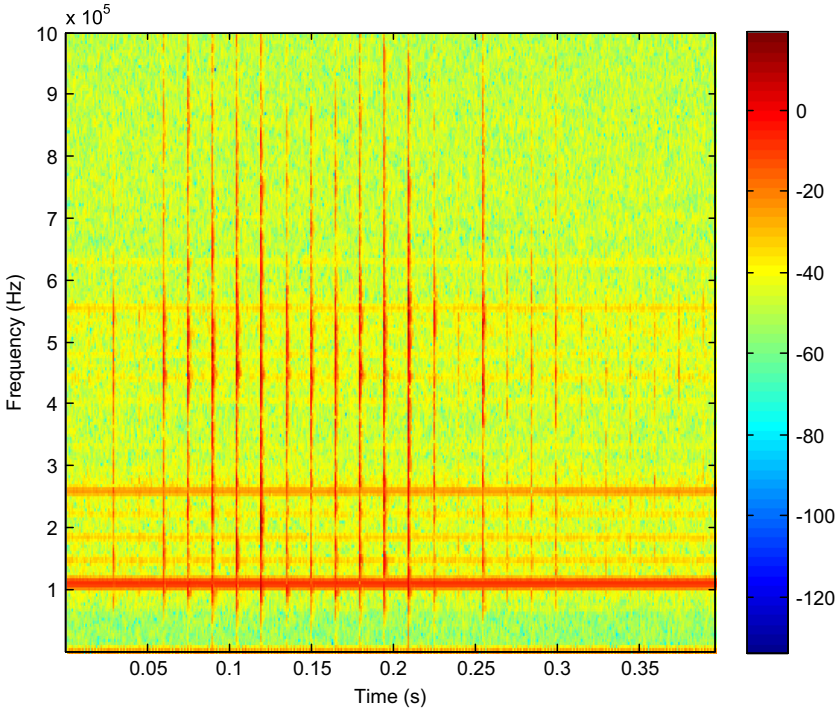

Fig. 10 STFT for the Titanium-64 material during test 54

obtained by the Titanium-64 tests are based on having a lower hardness level, which is significant of less material resistance, thus allowing more plastic deformation (see Table 1).

Figures 7 and 8 look at the STFT representations of Figs. 3 and 4, respectively, where the same signals are translated into the frequency and time domains. From the intensities recorded, it can be appreciated how the grit to material interactions change. In Fig. 7 and the beginning and end of Fig. 8, the very minute intensities can be seen, significant to approaching touch and actual touch (rubbing). Both figures look at the STFT reference to the CMSX4 SG tests. Figure 8 starts off showing actual

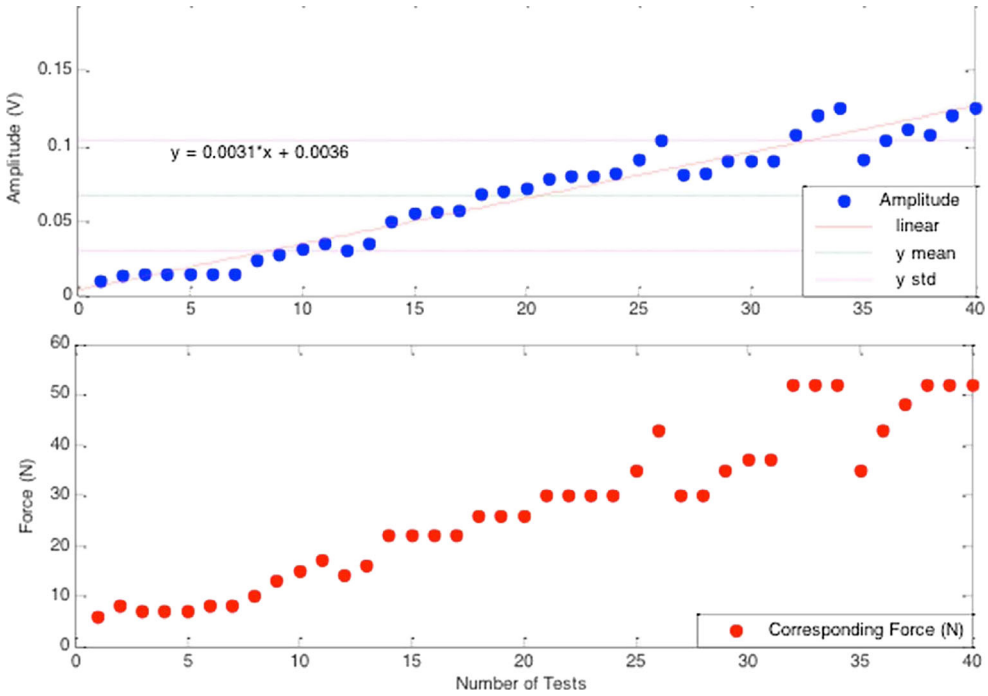

Fig. 11 AE vs force relationship in SG tests

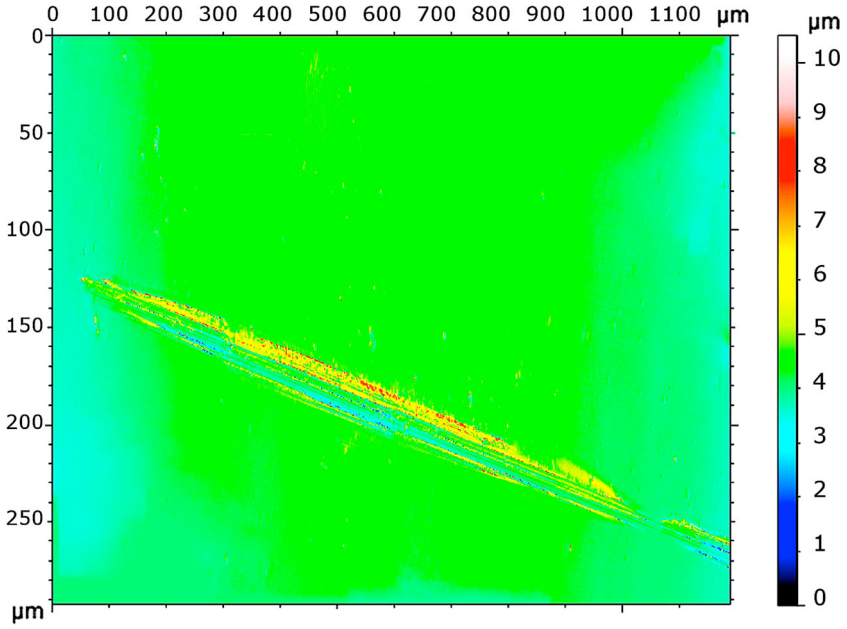

Fig. 12 SG4 test 212 hit 17, 3D Mountains scratch

touch (rubbing) tending towards ploughing and ultimately, the cutting phenomenon.

Figures 9 and 10 look at the STFT representations of Figs. 5 and 6, respectively, for the SG tests using the Titanium-64 material samples. Again, the intensities can be appreciated in terms of the approaching grit/workpiece interactions. With the very minute intensities, significant to approaching touch and actual touch (rubbing) displayed in Figs. 9 and 10 shows the same phenomenon as Figs. 7 and 8, albeit using the material Titanium-64.

Figure 11 was used from previous SG trials, where a relationship was found between AE and SG scratch, tested on the CMSX4 material samples. However, the load cell was located immediately below for the carried out scratch trials. Such information gives an indication of the recorded AE levels against that of force. Note that the CMSX4-extracted signal was normalised taking into account the different distances from each sensor to the scratch, while in the Titanium-64 case, this was unnecessary since the sensors were equidistant to the scratch.

When the process of grit to workpiece interaction occurs, AE is emitted as a material stress release process. This emitted AE during the scratch may come from elastic or plastic shear stress due to material removal or deformation mechanisms.

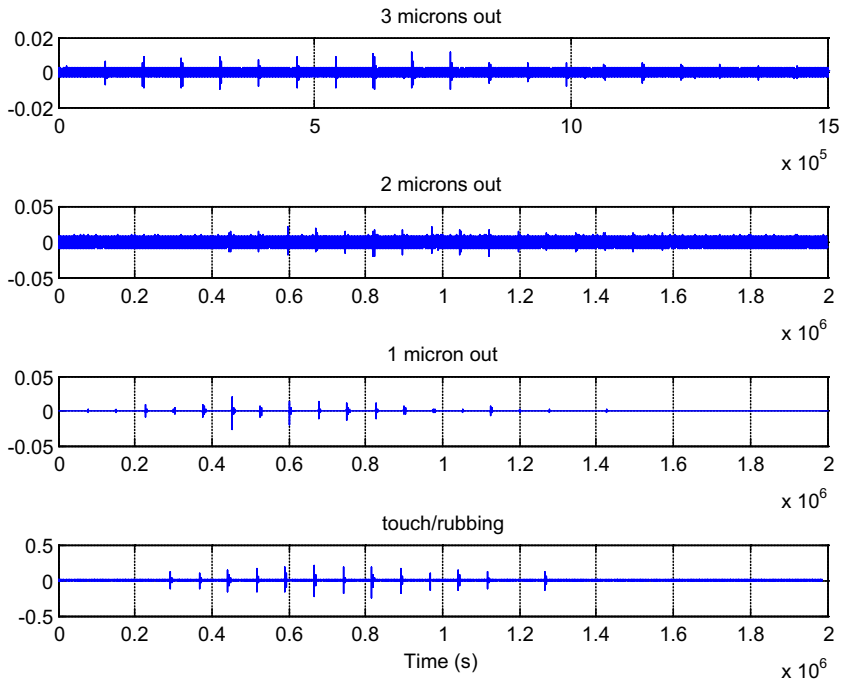

Fig. 13 Time AE signal for approaching touch and touch for Titanium-64 material

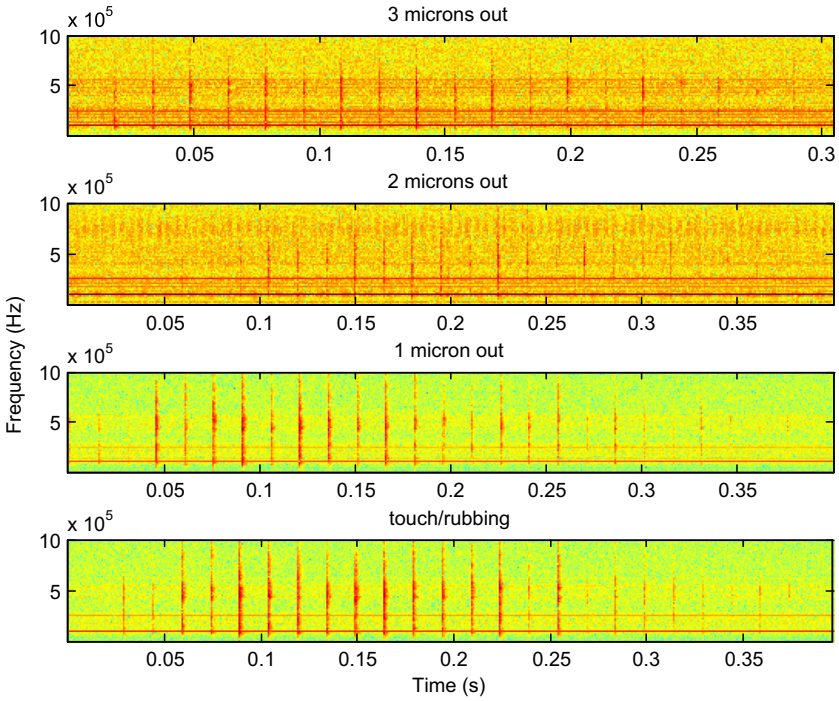

Fig. 14 STFT AE signal for approaching touch and touch for Titanium-64 material

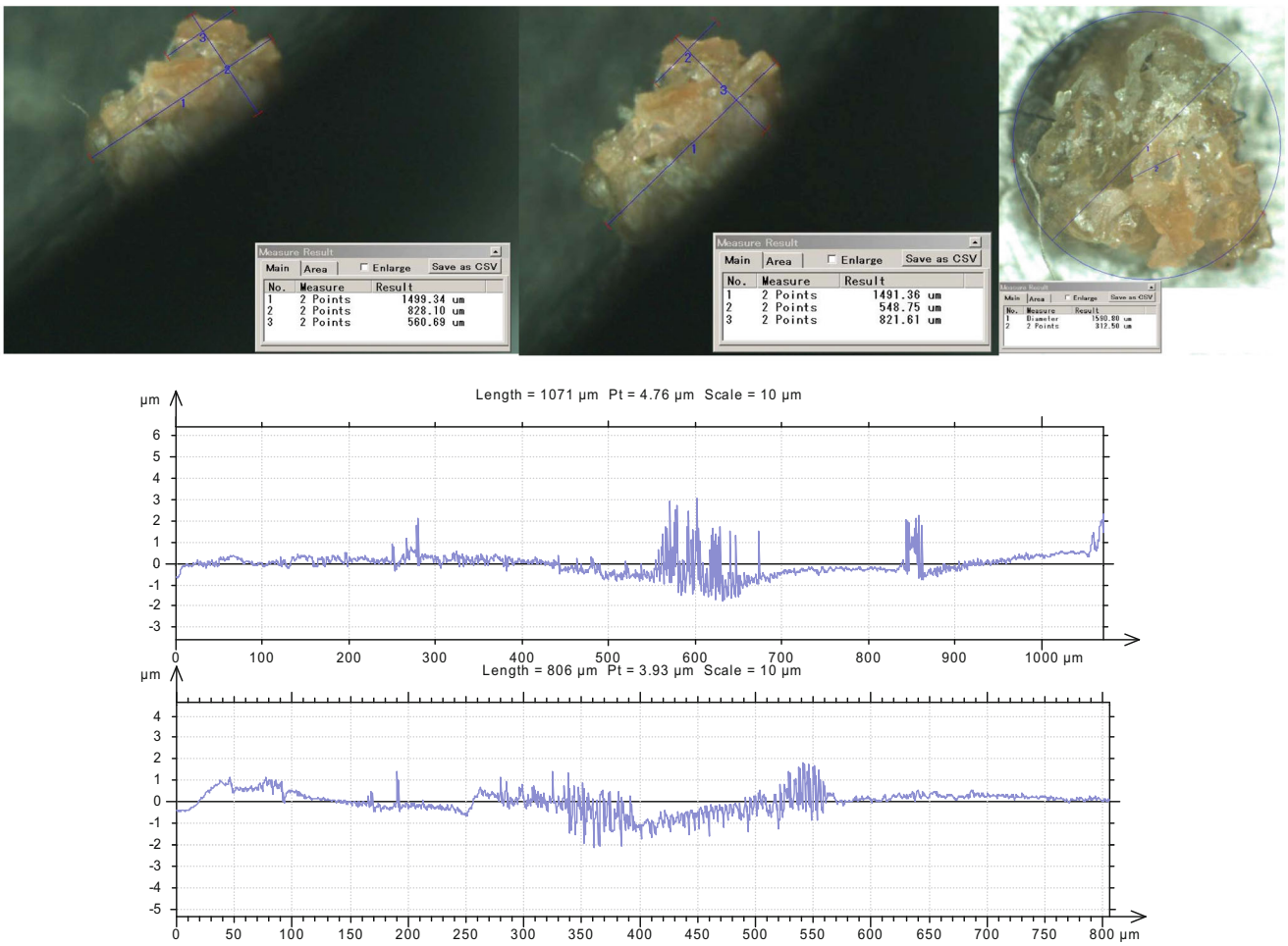

Fig. 15 *Top left*: side view grit before test 2 scratches, *top middle*: side view grit after test 2 scratches, *top right*: plan view of grit after test 2 scratches, middle cut profile of initial scratches and *below*: cut profile of final scratches

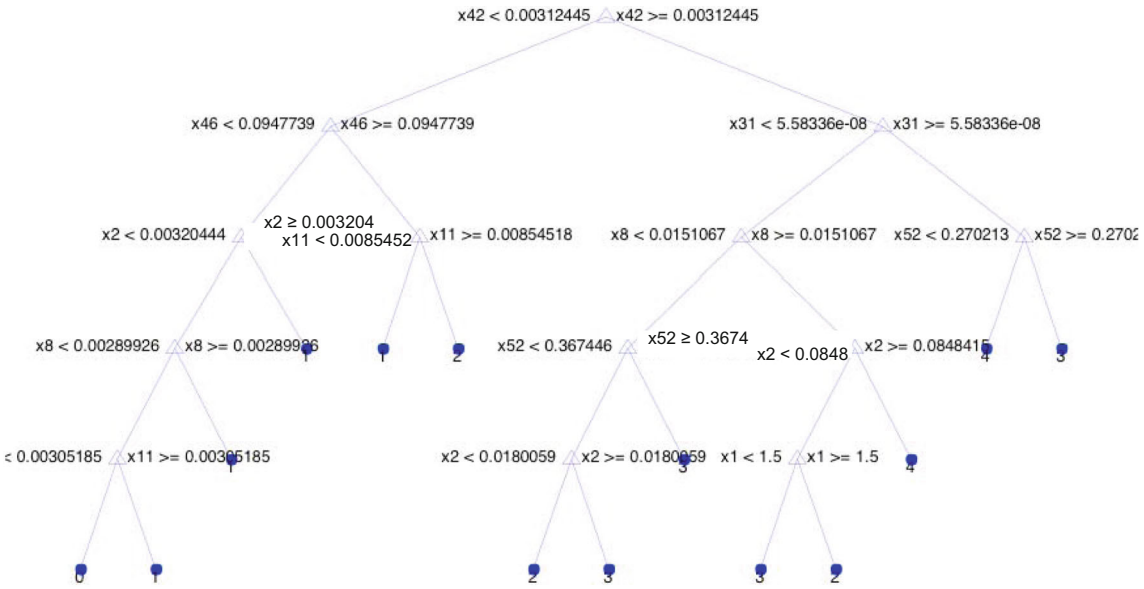

Fig. 16 Output classification for full tree CART rules for CMSX4 material

The process of identification between the various mechanics of different material removal rates or increasing DOC can be found in similar research on cutting, ploughing and rubbing performed in [23]. Such mechanics are significant to the amount of material removed, where cutting has the most material, then ploughing and, finally, rubbing, where no material is removed and the phenomena is significant to touch. Both sensors used not only verify each other but can also triangulate the position where the phenomena are occurring based on their intensities.

Pencil break tests used in [13] and [24] also displayed a large response time to what can only be described as a micro-second fracture [23]. The Hsu–Heilsen pencil break calibration method is an international best practice where the breaking of a high polymer graphite pencil provides a localised AE burst, which is analogous to a broadband step-release transient wave. This extracted wave can be assumed as the sensor's characteristic amplitude and frequency response. This method of AE sensor calibration has been used in grinding technologies before in [21] and [25]. Important points to take here are that we can calibrate the AE energy against force and, on a daily basis, obtain a normalised quantity to compare measurements carried out under different environmental conditions or

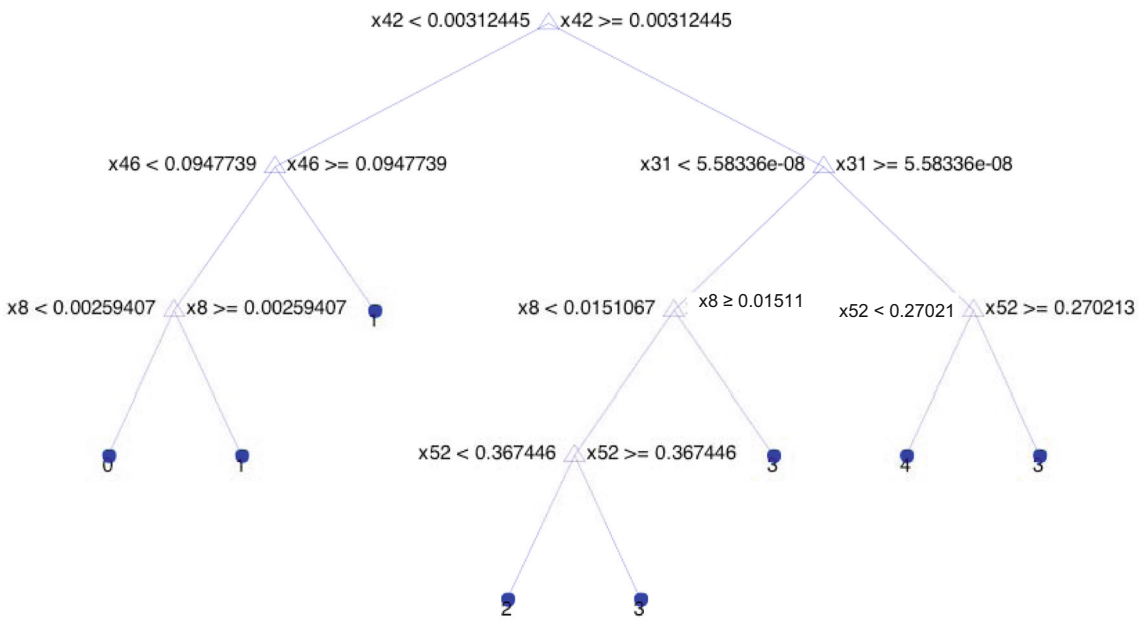

Fig. 17 Output classification for full tree CART rules for Tit-64 material

Table 2 NN parameters for classification

Parameter	Value
Hidden layers	2
Input size	72
Transfer function	Tan-sigmoid
Output function	Linear
Epochs	1000 for (1)
	Time: 20 min.
Learning rule	Gradient descent with adaptative learning rate (traingda)
Learning rate	0.1^{-9}
Momentum	0.7
NN training performance (SSE)	3.79×10^{-3}
Training	272 cases comprising all 5 phenomena

even different fixture damping mechanisms. Looking at Fig. 12, it was noticed that the changing features of AE signal intensities were similar to the shape of the produced grit scratch.

Therefore, AE amplitude can correlate, in both time and frequency domains, to different levels of grit/workpiece interaction, starting with levels of approaching touch.

With the different energy signatures occurring from the SG interacting within the workpiece, the STFT provides a good solution for separating different material removal mechanisms for precision control (energy consumed during surface deformation). However, in the rubbing case, there is only surface friction [26]. Therefore, this suggests that different AE signatures should be apparent between the two different phenomena (approaching touch and touch). Further to this, approaching touch has very different characteristics yet tending towards touch signatures, albeit with lower intensities.

Figures 13 and 14 show the different levels of approaching touch significant of sensor detection from 3 μm to actual touch. Figure 13 displays the time-based AE signatures 3 μm to touch and Fig. 14 displays the corresponding STFT plots. Further to Fig. 13, it can be seen that as the phenomena of grit and workpiece get closer, so do the intensities of AE increase.

It is often overlooked that grit too has wear mechanisms associated with SG scratch tests. The extracted AE is predominately based on the scratch deformation; however, there are grit mechanisms where such phenomena is difficult to distinguish from AE signals. Looking at Fig. 15, it can be seen that before and after the CMSX4 SG scratches 2 images (see Fig. 15 top left and centre), the grit wore more flat where 7 μm of material was removed in the form of removed chip. It was also noticed that at the beginning of the scratches (1–11), there is more of the obtained area of scratch cross section and less

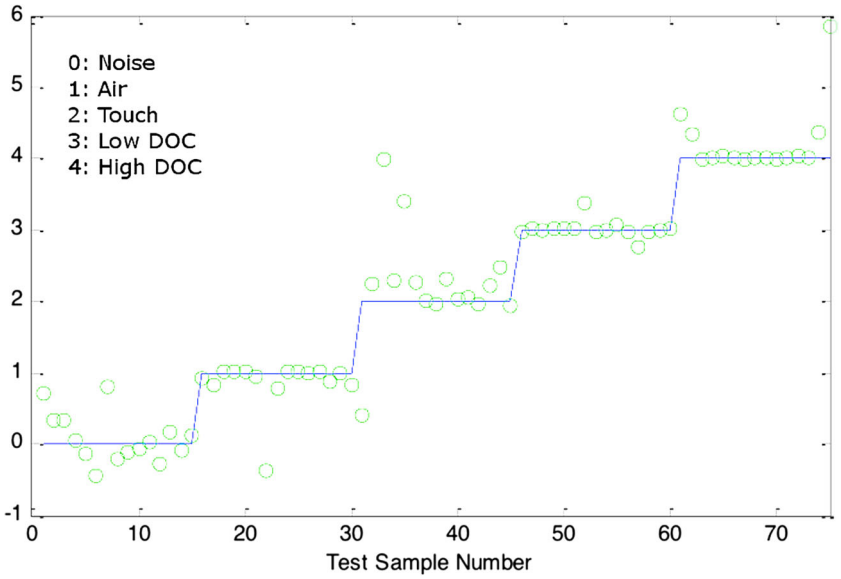

Fig. 18 Output classification for NN (CART rules verification). Results with 50 % of unseen and 50 % seen data

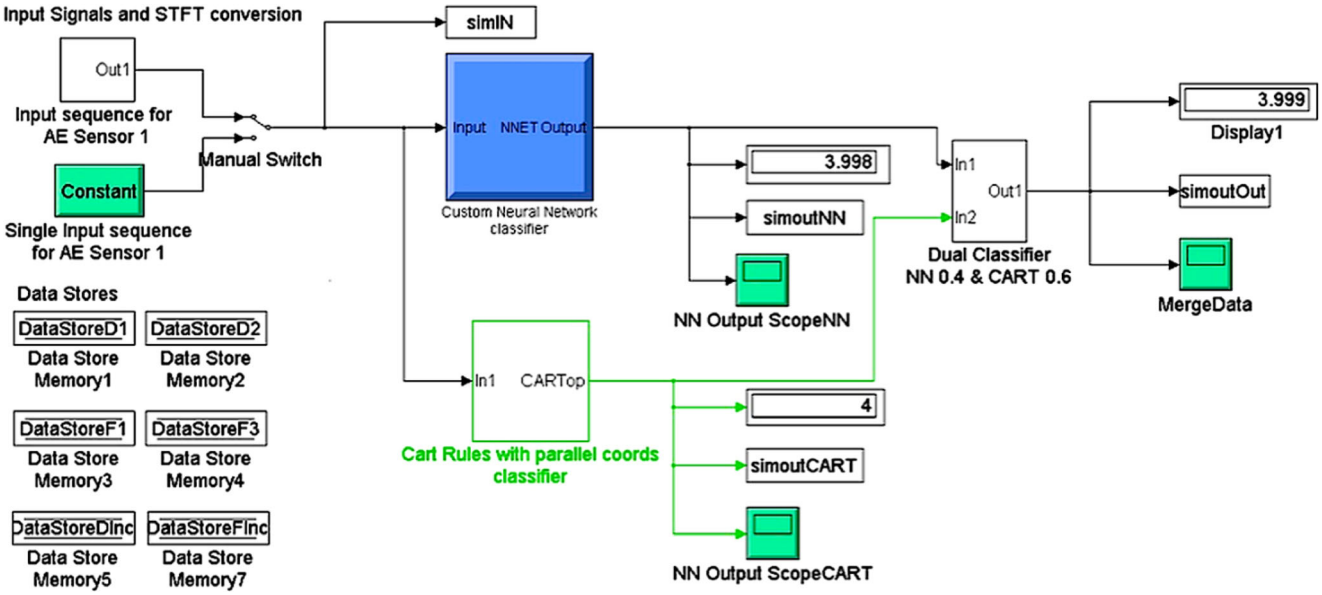

Fig. 19 Simulation for control of micron precision phenomena using a NN and CART rules

material pileup (see Fig. 15, middle for longitude corresponding scratch profile) whereas towards the end of the scratches (15–21), the same DOC is maintained albeit with a reduced cross-sectional area and higher material pileup (towards the end of the individual scratch length) which is due to the increased grit wear flat (see Fig. 15, bottom for longitude corresponding scratch profile). Looking at Fig. 15 top right, the plan view of the grit gives the diameter of the grit material as well as identified chip removal from SG process. The Titanium-64 grit wear mechanisms results were similar to CMSX4; however, over a similar range of scratches, less wear was recorded: 4.5 μm, and such results are consistent with other work [27–29]. Looking at the images of Fig. 15, there were no micro chippings or fractures recorded, only wear which is consistent with the scratch and grit profiles and further verifies the concept for approaching touch control.

6 Classification of micron-phenomena

Within this section, both CART and NN results are provided. Section 6.1 displays the CART rules, based on *if* and *elseif* and its associated results. Section 6.2 displays the architecture and results of the NN classifier as a backup verification method.

6.1 CART results

The following tree listing displays the full rule-set achieved from CART for controlling micron precision phenomena.

The results achieved by this method give an easily transferable rule set for use in an embedded controller. Moreover, it is also transparent in terms of which features of the signal are more salient than others. The output results were based on 272 test cases for establishing the rules, then tested against 75 cases with 50 % of the data relating to unseen cases. The classification accuracy obtained was 96 %, which gives a high confidence as a method for the control of precision machining using AE signals. Figures 16 and 17 give output CART rules for CMSX4 and Titanium-64 SG tests, respectively.

6.2 NN results, verifying CART classifications

The following results are based on NN classification, which are used to support and verify the results obtained by CART. The second verifier classifier used is the dual classification system within the embedded controller on section 7 which is a NN to ensure a more robust decision-orientated system and is less sensitive to outliers as seen with a single classifier system.

The NN architecture that was used in this section is displayed in Table 2. The results achieved by this method verify the CART rules, see Fig. 18, which is representative of the same test and data set used during the CART classification results. CART rules were chosen over NNs as the NN output is considered as an output from a black box classifier, thus non-transparent in showing the transient salient features. The output results were based on 272 test cases for establishing the rules and then tested against 75 cases with 50 % of the data relating to unseen cases. The classification accuracy obtained was 84 %, which again gives a high confidence albeit less than the accuracy given by the CART rules, which is less susceptible to achieving local minima and sensitive towards outliers as they determine their classification based on segregating different portions of the overall data set (similar to fuzzy clustering) and not summated output that is tested

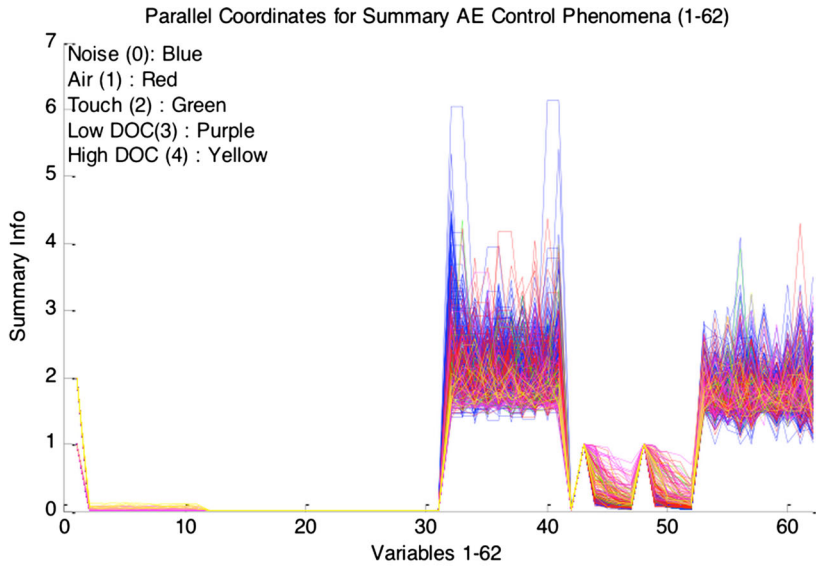

(a) Parallel coordinates of summary data set variables 1 to 62.

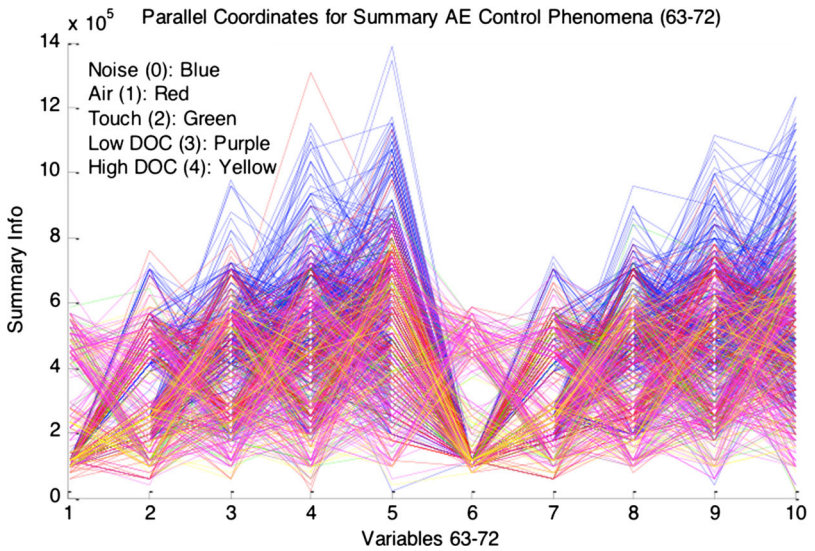

(b) Parallel coordinates of summary data set variables 63 to 72.

Fig. 20 Classification results for summarised data set where *0* is noise, *1* is air, *2* touch, *3* is low DOC and *4* is high DOC. **a** Parallel coordinates of summary data set variables 1 to 62. **b** Parallel coordinates of summary data set variables 63 to 72

against the overall error amounts reference to actual minus desired output (back propagation rule).

In discussing the obtained results further, if the AE sensor is set up and calibrated correctly, then this sensor can be used as a sensitive accurate sensing capability. A second sensor is usually added to the sensing capability due to the lack of standardisation based on its characteristic sensitive changing nature. Nevertheless, if measures are taken to ensure consistent stable results, then AE can be used as a single entity.

Looking at Figs. 13 and 14, some AE signatures are more intense than others; this is due to the profile grit shape and the corresponding workpiece surface profile where peaks and troughs can be identified. This is where AE can be used in 3D 3 sensors or more to give in situ scanning capabilities ensuring greater precision. The size of the grit can change from increased wear mechanisms of material interactions; however, the grit, which was of size 60 with manufacturing information Tyrolit XA 60 E13 VIPER grinding wheel is an open, soft-medium grade grit, which can be intensionally changed based on a laser ablation process [30]. Such tailored grit changes can be used for specialist micron geometries. It should also be noted the SNR are smaller for approaching touch compared to actual touch and increasing plastic deformation.

7 Real-time controller of micron phenomena

Figure 19 displays the top-level simulation for the proposed real-time precision machining controller. The input sequence for sensor 1 is a block, where 14 more signals varying in

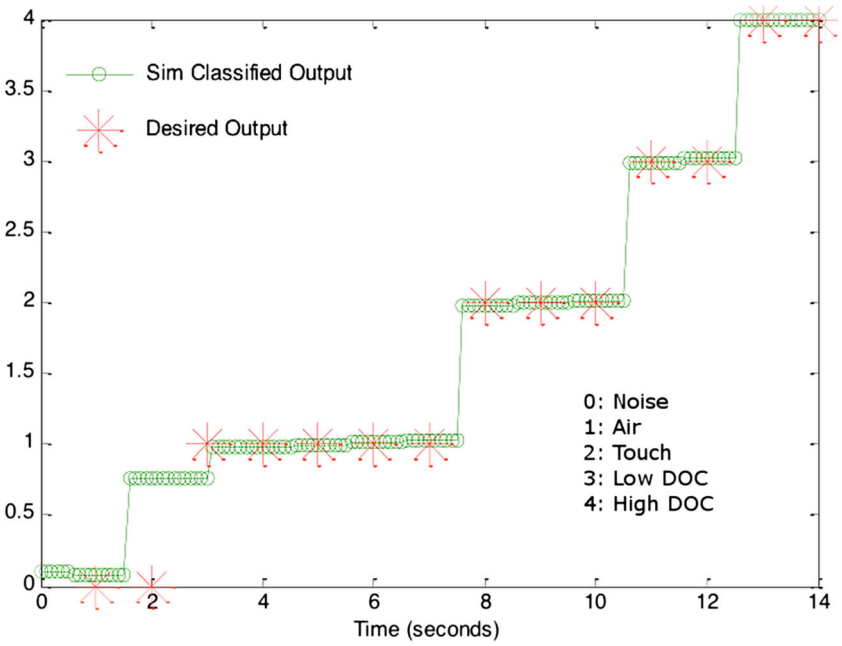

Fig. 21 Output from the merged CART and NN classification giving precision AE control

intensity from noise to high DOC (cutting plastic deformation) are applied sequentially to the double-decision classifier system. Within this block, the data is converted from the raw AE signal to a rich summarised data set based on the five maximum and five minimum peaks, their corresponding time-step, the kurtosis of each peak and, finally, the added ten STFT calculated peaks.

This summarised data is based on a 300-point-length window sequentially concatenated across the whole extracted signal of interest. Once summarised, the data is sent to both classifiers (CART and NN) to determine whether they are noise (0), approaching touch (1), touch (2), low DOC (3) or high DOC (4).

To obtain such high classifications as seen in section 6.1, the rules need to be translated in the correct fashion as well as in the correct order. This ordering can give rise to problems in terms of the correct priorities and support against any ambiguities (as found between noise, approaching touch and touch). Parallel coordinates (as seen in Fig. 20) are used to make pre-segmentations and in collaboration with the translated CART rules affords a robust classification capability.

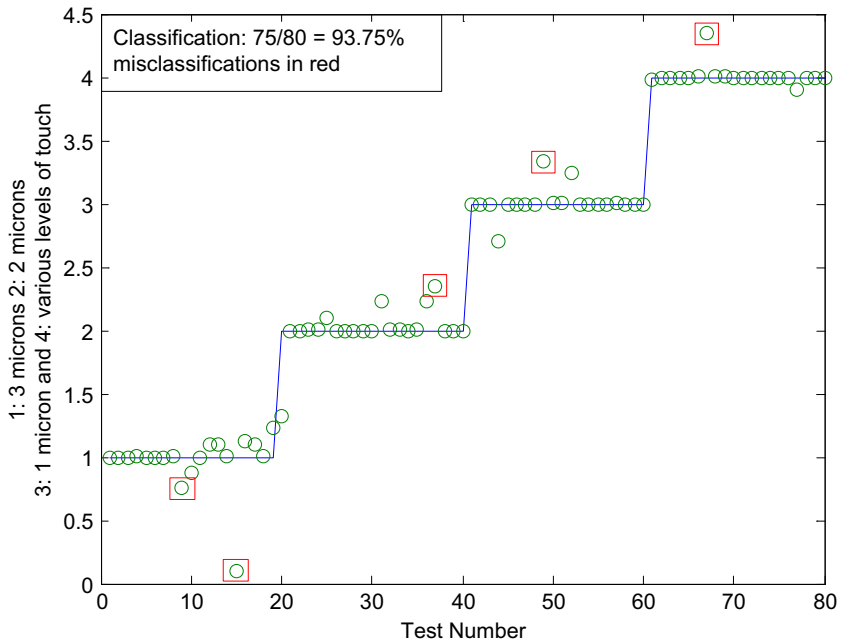

Fig. 22 Static output test from the merged CART and NN classification giving approaching touch control

Figure 21 displays the output of the merged classifiers giving the accurate precision control, and the only misclassifications were seen between the 0 and 1 phenomena transition; however, as such sources are changing in terms of micron perturbations and increasing as the phenomena changes from approaching touch to touch, such transitions are expected. More importantly, the classification of phenomena 1 and 2, relating to near touch and actual touch, respectively, gives a good account and pertinent to the work discussed in this paper. Figure 22 displays a static output test for approaching touch and touch which is considered key to the work presented here.

The extra results displayed in Figs. 13 and 14 can easily be implemented in this model however have to be driven independently as more misclassification will be apparent with similar added dimensional data corresponding to differing output states. Having segmented intelligence is the preferred route when requiring high levels of robustness and accuracy (see Figs. 21 and 22 for examples of this). To ensure a more robust system the RMS value can be added to ensure data is less reactive to sudden change such as spikes seen with sensitive peak to peak data sets.

8 Conclusions

The method of precision control through AE was made robust while using a summarised data extraction technique on the raw time extracted signal and its corresponding STFT frequency analysis. When using such reduced data, the grinding process on both materials tested can be controlled in terms of micro precision. The dynamic control is provided from sensing distances of 3-μm away from the surface to actual touch. The work discussed here shows the differences in AE intensities (time and STFT) which is significant of different SNRs which can also be used for rapid real-time control environments.

Such micron precision control is becoming more important as geometrical accuracies become more demanding (turbine root-forms now have 0.5-μm tolerances) and micro applications are becoming more common to industry (e.g. micro pumps seen in medical devices). Moreover, it becomes almost impossible to see if accuracies have been achieved unless a high-powered microscope is used offline. In addition, there are many control problems investigating industrial robots to move large weights with precision, and the work presented here can be extended to such scenarios. Lastly, the methodology presented here looks at AE sensor control used in situ, which has direct usability and transferability to industry. The results displayed by the CART rules give a robust account for use in real-time systems. Coupled with NNs, outliers and misrepresented structures are considered less of a problem, giving further confidence to reliability and confident industrial use.

References

1. Hatano H, Chaya T, Watanabe S, Jinbo K (1998) Reciprocity calibration of impulse response of acoustic emission transducers. IEEE Trans Ultrason, Ferro Elec Freq Control 45(5 [12]):1221–1228
2. Griffin J, Chen X (2014) Real-time simulation of neural network classifications from characteristics emitted by acoustic emission during horizontal single grit scratch tests. J Intell Manuf. Online, ISSN 1572–8145
3. Deshpande A and Pieper R Legacy machine monitoring using power signals analysis. Procs ASME Int Manuf Sci Eng Conf, MSEC., Oregon, USA, pp. 1–8, 2011.
4. Burke L, Rangwala S (1991) Tool condition monitoring in metal cutting: a neural network approach. J Intell Manuf 2:269–280
5. Jemielniak K, Kwiatkowski L, Wrzosek P (1998) Diagnosis of tool wear based on cutting forces and acoustic emission measures as inputs to a neural network. J Intell Manuf 9:447–455
6. Xiaoli L, Yingxue Y, Zhejun Y (1997) Online tool condition monitoring system with wavelet fuzzy neural network. J Intell Manuf 8: 271–276
7. Venkatesh K, Zhou M, Caudill R (1997) Design of a neural network for tool wear monitoring. J Intell Manuf 9:281–287
8. Sharma V, Dhiman S, Sehgal R, Sharma S (2008) Estimation of cutting forces and surface roughness for hard turning using neural networks. J Intell Manuf 8:215–226
9. Ren Q, Balazinski M, Baron L (2012) Fuzzy identification of cutting acoustic emission with extended subtractive cluster analysis. Nonlinear Dyn 67(4):2599–2608
10. Ren Q, Balazinski M, Jemielniak K, Baron L, Achiche S (2013) Experimental and fuzzy modelling analysis on dynamic cutting force in micro milling. Soft Comput 17:1687–1697
11. Ren Q, Baron L, Balazinski M, Jemielniak K, Botez R, Achiche S (2014) Type-2 fuzzy tool condition monitoring system based on acoustic emission in micromilling. Inf Sci 255:121–134
12. Warnecke G, Kluge R (1998) Control of tolerances in turning by predictive control with neural networks. J Intell Manuf 9:281–287
13. Barbezat M, Brunner AJ, Flueler P, Huber C, Kornmann X (2004) Acoustic emission sensor properties of active fibre composite elements compared with commercial acoustic emission sensors. Sensors Actuators 114:13–20
14. Godin N, Huguet S, Gaertner R, Salmon L (2004) Clustering of acoustic emission signals collected using tensile tests on unidirectional glass/polyester composite using supervised and unsupervised classifiers. NDT&T Int 37(4):253–264
15. Li X, Zhejun Y (1998) Tool wear monitoring with wavelet packet transform-fuzzy clustering method. Wear 219(2):145–154
16. Breiman L, Friedman J, Olshen R, Stone C (1984) Classification and regression trees. CRC Press
17. Hartigan J (1985) Statistical theory in clustering. J Classif 2(1):63–76
18. Coppersmith D, Hong SJ, Hosking JR (1999) Partitioning nominal attributes in decision tree. Data Min Knowl Disc 3(2):197–217
19. Sick B (2002) On-line and indirect tool wear monitoring in turning with artificial neural networks: a review of more than a decade of research. Mech Syst Signal Process 16(4):487–546
20. Ozel T, Karpat Y (2005) Predictive modeling of surface roughness and tool wear in hard turning using regression and neural networks. Int J Mach Tools Manuf 45(4):467–479
21. Griffin J, Chen X (2014) Real-time fuzzy-clustering and CART rules classification of the characteristics of emitted acoustic emission during horizontal single-grit scratch tests. Int. J Advan Manuf Tech. 1–22
22. Chen X, Griffin J, Liu Q (2007) Mechanical and thermal behaviours of grinding acoustic emission. Int JManuf Tech Manag 12(1–39): 184–199

23. Griffin J, Chen X (2009) Characteristics of the acoustic emission during horizontal single grit scratch tests part I. Characteristics and identification. Int. J Abrasive Tech Special Issue Micro/Meso Mech Manuf (M4 Process) 1(4)
24. Boczar T, Marcin L (2006) Time-frequency analysis of the calibrating signals generated in the Hsu-Nielsen system. Phys Chem Solid State 7(3):585–588
25. Hwang TW, Whitenton EP, Hsu NN, Blessing GV, Evans CJ (2000) Acoustic emission monitoring of high speed grinding silicon nitride. Ultrasonics 38(1):614–619
26. Kalpakjian S, Schmid SR (2003) Manufacturing process for engineering materials. Prentice Hall, ISBN 0-13-040871-9, pp. 510–520
27. Opoz TT, Chen X (2010) An investigation of the rubbing and ploughing in single grain grinding using finite element method, in: Proceedings of the 8th International Conference on Manufacturing Research, Durham, UK, pp. 256–261
28. Matsuo S, Toyoura E, Oshima Y, Ohbuchi Y (1989) Effect of grain shape on cutting force in super abrasive single-grit tests. CIRP Annals—Manufacturing Technology 38: 323–326
29. Park HW, Liang SY, Chen R (2007) Micro grinding force predictive modelling based on microscale single grain interaction analysis. Int J Manuf Technol Manag 12:25–38
30. Gilbert D, Stoesslein M, Axinte D, Butler-Smith P, Kell J (2014) A time based method for predicting the workpiece surface micro-topography under pulsed laser ablation. J Mater Process Technol 214(12):3077–3088